Knee Cartilage Segmentation using Improved U-Net

Nawaf Waqas[1], Sairul Izwan Safie[2], Kushsairy Abdul Kadir[3], Sheroz Khan[4]
Universiti Kuala Lumpur, Malaysian Institute of Industrial Technology, Johor, Malaysia[1,2]
Universiti Kuala Lumpur, British Malaysian Institute, Selangor, Malaysia[3]
Department of Electrical Engineering, Onaizah College of Engineering and Information Technology
PO Box 2053, Al-Qassim 56447, Saudi Arabia[4]

***Abstract*—Patello-femoral joint stability is a complex problem and requires detailed anatomic parametric study for knowing the associated breakdowns of knee cartilage. Osteoarthritis is one of the main disorders, which disrupt the normal bio-mechanics and stability of the patello-femoral joint and for diagnosing osteoarthritis radiologists needs a lot of time to diagnose it. An improved network called PSU-Net is proposed for the automatic segmentation of femoral, tibia, and patella cartilage in knee MR images. The model utilizes a Squeeze and Excitation block with residual connection for effective feature learning that helps in learning imbalance anatomical structure between background, bone areas and cartilage. The severity of knee cartilage is measured through the Kellgren and Lawrence (KL) grading system by radiologists. Also, updated weighted loss function is used during training to optimize the model and improve cartilage segmentation. Results demonstrate that PSU-Net can accurately and quickly identify cartilages compared to the traditional procedures, aiding in the treatment planning in a very short amount of time. Future work will involve the use of augmentation methods and also use this architecture as a generator model for generative adversarial network to improve performance further. The utility of this work will help in analyzing the anatomy of the human knee by the radiologists in short amount of time that may prove helpful to standardize and automate patello-femoral measurements in diverse patient populations.**

Keywords*—Knee image segmentation; U-Net; loss function; squeeze and excitation

I. Introduction

Patello-femoral joint stability depend on the knee. The patello-femoral joint is formed between the patella (kneecap) and the femur (thigh bone). It is a complex joint that allows for the movement of the patella during knee flexion and extension. The knee is known as the largest joint in the human body [1]. One of the important components in the knee joint is the cartilage. Cartilage is fine, rubbery, and flexible tissue that covers the surface of bones, which can be found throughout the body. Cartilage helps to reduce friction by acting as a cushion and lubricant between the joints. However, repeated bio-mechanical force or a sudden impact will cause the knee cartilage to experience wears down or tear, leaving the rough bone surface exposed to each other resulting the friction in between the constituent structures making the joint [2]. This situation is called damaged cartilage. Prolonged damage over the time will lead to the happening of Knee Osteoarthritis (KOA) with long-term irreversible effects on normal knee function. Eventually, the disease would lead to permanent physical disability.

KOA is a form of arthritis characterized by inflammation, degradation, and ultimate loss of cartilage in joints, most often affecting the knee's major weight-bearing joint [3]. KOA can be classified according to degradation severity. In 1961, WHO has accepted the Kellgren and Lawrence (KL) grading system as a standardized way to identify and grade the severity of (KOA) [4]. The grading scheme classified KOA into five different levels by assigning a grade from 0 to 4 [5].

Knee osteoarthritis (KOA) can be categorized into different severity levels based on magnetic resonance (MR) images. In the normal knee (KL 0 grade), there is no visible damage. In mild KOA (KL 1 grade), minor loss is observed in the femoral cartilage. Mild KOA (KL 2 grade) shows some loss in bone density in the femoral and patella cartilage. Severe KOA (KL 3 grade) exhibits tearing in the femoral cartilage, while in the most severe stage (KL 4 grade), almost the entire femoral cartilage seems to have worn down, exposing the bone and causing tissue signal inhomogeneity.

Knee cartilage segmentation plays a crucial role in diagnosing KOA. By accurately identifying and delineating the cartilage boundaries from medical imaging such as MRI, segmentation techniques enable quantification and assessment of cartilage health. This information helps in evaluating the severity of osteoarthritis, tracking disease progression, and guiding timely treatment decisions. Additionally, precise cartilage segmentation aids in detecting early cartilage degeneration and monitoring the effectiveness of interventions or therapies. Overall, knee cartilage segmentation plays a vital role in providing objective and quantitative measurements for diagnosing and managing osteoarthritis.

The remaining paper is organized with Section II explaining the related work, Section III describes the methodology, the Experiment work is presented in Section IV. Section V gives evaluation metrics and results and discussions are given in Section VI before Section VII concludes the paper.

II. Related Work

Segmentation of cartilage can be performed manually or by using computational approaches. Computational approaches can be classified into two which is semi-automatic or automatic methods. Manual segmentation of cartilage results usually gives more reliable outcomes compared to computational approaches. In a manual approach, cartilage will be segmented slice by slice from 2D MR images. Although manual segmentation outcome has high accuracy and sensitivity [6] and has been widely used to evaluate the performance of semi-automatic or automatic segmentation methods, it requires extra effort to the user and is time-consuming. This may result in inter and intra observer variability between the experts [7].

The region-based segmentation approaches have been classified under semi-automatic and conventional segmentation approaches. Based on [8], [9] this approach use the concept of exploiting the homogeneity property values of neighboring pixels such as grey-level intensity, texture, and edge [10]. Often, the initialisation point of segmentation or also known as seed points, $S_i = \{S_{1,}, S_2 \ldots, S_n\}$ will be manually placed by a user. After placing the seed points, the algorithm will next begin to search for homogeneous pixels in neighbouring pixels [11] and keep updating the corresponding region's mean and expanding until the similarity requirement is met. In equation (1), let T represent the set of all pixels that adjacent to at least one of the pixels in Si where nb(x) denotes the set of nearest neighbours pixel of x.

$$T = \left\{ x \notin \bigcup_{i=1}^{n} S_i \,\middle|\, nb(x) \cap \bigcup_{i=1}^{n} S_i \neq \emptyset \right\} \tag{1}$$

This approach has been widely used in the past two decades. However, the traditional region-growing approach is incapable to deal with the inhomogeneous image quality, especially for knee MR images. With this limitation, further research has been conducted by combining this approach with other image-processing approaches to achieve robust segmentation results. The author in [12] proposed a region growth approach by introducing the binary-class intensity-based local clustering to segment knee cartilage from a background image. Binary-class intensity-based local clustering is a voxel labeling of cartilage or non-cartilage. This approach was introduced to differentiate the class of unlabelled areas based on the distance to the knee bone and the contrast of the boundaries area. Finally, a 3D cartilage model was generated to tackle the issue of intensity inhomogeneity. The authors in [13], [14] performed a knee cartilage segmentation model based on a multistage region growth approach. This approach used a median filter to filter the image noise while edge detection and thresholding were used to remove the background image at the pre-processing stage. Next, the pre-segmentation stage by using region growth will take place. Output from this stage was bone and cartilage region mask. Finally, the bone region mask will be removed to leave out the cartilage.

Recently, there have been significant advancements in automatic biomedical image segmentation using deep neural network techniques [15], [16], [17]. In the context of segmenting knee joint structures, Burton et al. [18] initially employed two-dimensional (2D) tri-planar CNNs (axial, coronal, and sagittal planes) to classify pixel labels (background or tibial cartilage) by considering local image patches surrounding each pixel. However, Ronneberger et al. [19] identified two limitations with this approach: excessive redundancy and a trade-off between localization accuracy and the utilization of context. To address these issues, they proposed a dense prediction network called U-Net, which incorporated skip connections. This architecture encompassed both low-level and high-level features for voxel classification and was subsequently employed for knee joint segmentation by Liu et al. [20], Zhao et al. [21], and Ambellan et al. [22]. Generally, the U-Net employed pixel-wise or voxel-wise loss functions such as cross-entropy loss and dice loss. However, the resulting segmentation lacked spatial consistency [23]. The reason is that U-Net consists of only Convolution layers that suffer from the training-related issues of vanishing gradient and dead neurons considered as the main research gap being addressed in this work [24]. The main contribution of this paper is to propose an automatic deep learning segmentation model which can segment knee cartilage in the image efficiently and to do so we have introduced the proposed squeeze and excitation block in U-Net which will work alongside convolution layer of U-Net so that the architecture learning process goes smoothly. Additionally updated loss function is also used, which will help the proposed model to perform the task effectively.

III. Methodology

A. Proposed Squeeze and Excitation Block

The proposed Squeeze and Excitation Block, shown in Fig. 1, is composed of residual connection with Squeeze and Excitation block. The residual connection has been proven to be an effective way to overcome the problem of vanishing gradient when it comes to learning features in deep neural networks [25]. In [26], the authors have proposed SE-Net (Squeeze-and-Excitation networks), which is the ImageNet Challenge winner. The SE-Net adds the Attention mechanism to the feature channel dimension to learn the weight of each dimension through the loss function, and to learn the residual connection according to the importance of each channel feature. The image input after passing from convolution layers, delivers the feature map with size of H x W x C as the output. Then this feature map is passed colorred through Global pooling layer which reduces the size to 1 x 1 x C. Again, the output of global pooling layer is passed through fully connected layer and ReLU activation function thus reducing its channel by r as shown in Fig. 1. This process is known as the Squeeze operation. The output of Squeeze operation is then upsampled to 1 × 1 × C using another fully connected layer followed by sigmoid activation function, which gives weights for each of the channels, a process referred to as Excitation operation. Mathematically the Squeeze and Excitation operation can be expressed as in equations (2) to (5):

$$o_c = F_{sq}(x_c) = \frac{1}{H \times W} \sum_{h}^{H} \sum_{w}^{W} x_c(h, w) \tag{2}$$

Where F_{sq} represents squeezing operation, x_c represents feature map of X_m on the C dimension. H and W denotes the height and width of the feature map, h and w exemplify the abscissa and ordinate of a certain point on the feature map. The correlation between each feature channel is learned through the two fully connected layers and the ReLU activation function, and the correlation between the features is normalized by the Sigmoid function to obtain the weights for each feature channel, then these weights are multiplied by the input feature channel.

$$t_c = F_{\text{ex}}(o_c) = \text{Sigmoid}\left(W_2\left(\text{RELU}\left(W_1\left(o_c\right)\right)\right)\right) \tag{3}$$

$$\bar{x} = F_{\text{scale}}\ (x_c * t_c) \tag{4}$$

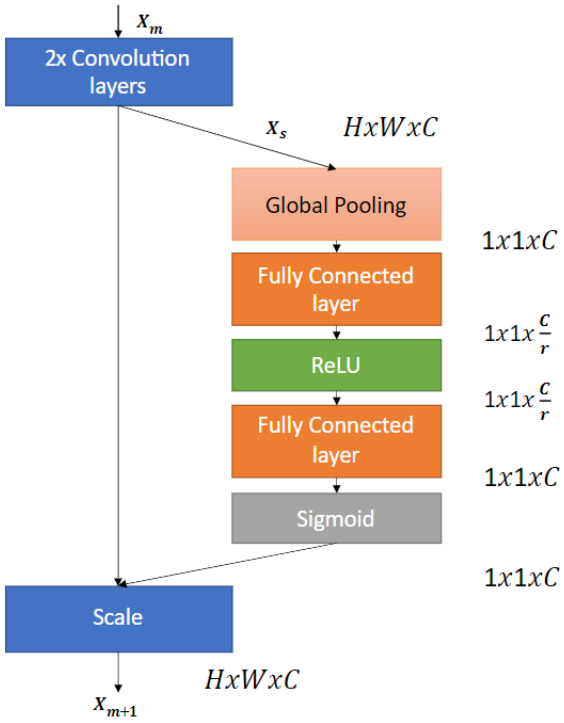

Fig. 1. Proposed squeeze and excitation block.

Where F_{ex} indicates an excitation operation, W_1 and W_2 show weights of two fully connected layers.

$$X_{m+1} = \text{RELU}\left(\bar{x} + X_m\right) \tag{5}$$

X_m signifies the input to the proposed block. Squeeze and Excitation block will then be embedded into the residual connection to improve the residual characteristics of different channels according to the degree of importance that will help in learning ability.

B. PSU-Net

Fig. 2 and Fig. 3 show the U-Net and PSU-Net architecture to segment the knee image data in NRRD format. It has the same architecture as that of the standard U-Net in the Down-convolutional part; each layer is consisting of two convolution layers followed by the activation function and then the input is down-sampled by the Maxpool layer in two-layered step. In the Up-Convolutional part each input coming from bottleneck layer is then upsampled by 2 x 2 in a two-layered step, followed by two 3 x 3 convolution layers and then followed by an activation function. The bottleneck layer connects Down-Convolution part to the Up-Convolution part that helps in stabilizing training and transferring information from Down-Convolutional part to Up-Convolutional part. The last convolution layer helps in reducing the number of labels to three according to number of class in our dataset. The input to the model in our case is 384 x 384 x 1 pixels and our output size is 384 x 384 x 3 pixels in which the digit 3 represents the classes (femoral, tibia and patella). We also used Batch normalization before activation functions.

In PSU-NET the two convolution layers block in the Up-Convolutional part and Down-Convolutional parts are replaced by the proposed Squeeze and Excitation block as shown in Fig. 3. Each unit of Down-convolutional part includes a proposed Squeeze and Excitation Block to extract image features and a down-sampling layer. The down-sampling is done using maxpool layer. The channel size is reduced to half, each unit of Up-Convolutional part includes a proposed Squeeze and Excitation Block and an upsampling layer. Upsampling uses transposed convolution, the channel size is expanded by two times. The last layer consists of convolution layer that helps in reducing the number of class to three - the femoral, tibia and patella in our case.

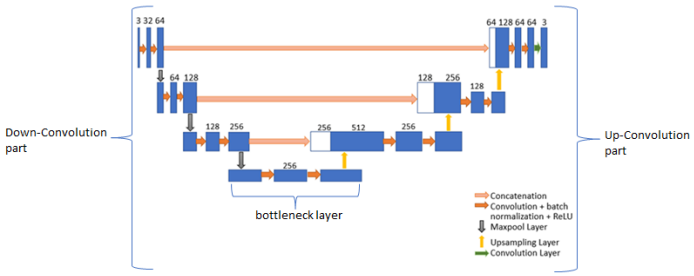

Fig. 2. Standard U-Net architecture.

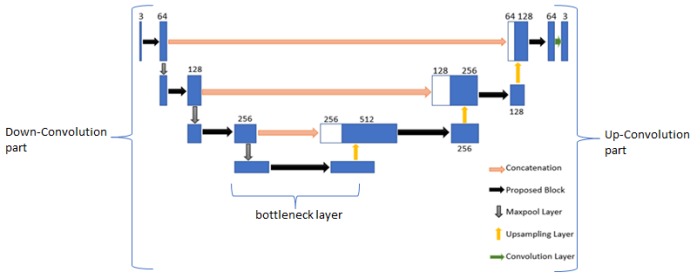

Fig. 3. PSU-Net architecture.

C. Loss Function

Knee image segmentation is done to divide the voxels of the cartilage of knee image into three classes: femoral, patella and tibia, using neural network. The pixel value of cartilages is approximately the same as different organs of the knee like meniscus etc. In order to make the neural network pay more attention to the cartilage, we give these pixels of cartilage greater weights to improve knee image segmentation. The weights can be expressed as in equation (6):

$$w_i = \frac{\left(\frac{1}{N_i}\right)^2}{\sum_{i=1}^{3}\left(\frac{1}{N_i}\right)^2} \tag{6}$$

Where w_i represents weight for each class, N_i is the total number of pixels in each class of the image. This paper uses a weighted multi-class loss function, which is a combination of Dice loss function and cross-entropy loss function to optimize the model. The formulas of the Dice loss function and the cross-entropy loss function are mathematically expressed in equation (7) and (8):

$$\text{loss}_{\text{Dice}} = 1 - \sum_{n=1}^{M}\sum_{i=1}^{C} w_i \frac{2 \cdot y_{ni} y'_{ni}}{y_{ni} + y'_{ni}} \tag{7}$$

$$\text{loss}_{\text{ce}} = -\sum_{n=1}^{M}\sum_{i=1}^{C} w_i y_{ni} \log\left(y'_{ni}\right) \tag{8}$$

Where M represents the total number of pixels in the image in a batch, C represents the class (femoral, patella, tibia), w_i Indicates the class weight obtained by using equation (6), and y_{ni} indicates the true probability value of the pixel belonging to class i, y'_{ni} represents the predicted probability value. Finally, the weighted loss function is as expressed in (9)

$$\text{Loss} = \lambda_1 \text{loss}_{\text{Dice}} + \lambda_2 \text{loss}_{\text{ce}} \tag{9}$$

IV. Experiment

A. Dataset

This study is carried out on 30 datasets from OAI [27] that can be found at http://oai.epi-ucsf.org/datarelease/About.asp, consisting of 160 slices each of Knee MR images. The datasets consist of various KL grades as listed in Table I. The KL grades are generally referred to in the medical images to reflect the damage of the cartilage in between joints. We labelled the cartilage of these 30 datasets using slicer [28] software. we divided these 30 datasets into 3 categories. 23 of training datsets, 5 of validation datasets and 2 of testing datasets.

TABLE I. Amount of Datasets for Various KL Grades

KL Grades	Dataset Numbers
0	8
1	4
2	5
3	6
4	7

B. Experimental Setup

The operating environment of this study is NVIDIA cuDNN7.5, CUDA10.0, Python 3.4, Anaconda, the hardware configuration is GTX 1060Ti GPU, 1 TB capacity hard disk, and the deep learning framework is built using Keras [29] with Tensorflow [30] as backend. Other libraries also used like SimpleITK [31], matplotlib [32], Scikit learn [33] and numpy [34] for reading, processing NRRD data and for other functions as well. The neural network learns the weights of each layer through training data and selects the optimal model through validation data to verify the performance of the model. Each epoch of learning randomly selects 80 percent of the training model from the training set, and the remaining 20 percent is used to verify the model to improve model learning ability. We have entered data in batches to reduce training time. In this study, the Adam optimization method is used to optimize the network, and the weighted joint loss function proposed in equation (9) is used to judge the training process of the network model. We have adjusted the parameters according to the training results, the parameter of loss function λ_1 and λ_2 Set to 0.3 and 0.7, respectively, set the training batch size to 2, and iterate the training data set for 50 epochs.

V. Evaluation Metrics

In order to quantitatively evaluate the segmentation performance of the algorithm in this paper, Dice coefficient (F1) and Intersection over union (IoU) are used as evaluation metrics, and these scores were measured by calculating the regional similarity between deep neural neural network predicted result and expert annotated result.

F1 score can be calculated by using following mathematical equation:

$$\text{F1} = \frac{2|A \cap B|}{|A| + |B|} \tag{10}$$

IoU score can be expressed mathematically as:

$$\text{IoU} = \frac{|A \cap B|}{|A \cup B|} \tag{11}$$

In above equation 10 and 11, A represents the ground truth of knee cartilage and B is the predicted segmentation result by segmentation models.

VI. Results and Discussion

Using the model of this paper to trained on 30 datasets of knee images to calculate the dice coefficient of our proposed model on training dataset and validation datasets during training of each epoch using dice coefficient and intersection over union. The box plot shown in Fig. 4 indicates the distribution of the dice coefficient of the femoral, tibia and patella cartilages during training. Usually, each of the datasets consists of 160 slices in which we have slices with cartilage and without cartilage. The average training dice coefficient of our proposed model during training on those slices which have femoral cartilage is up to 0.925, the average training dice coefficient on those segmented slice which has tibia cartilage is up to 0.945, and the average training dice coefficient on those slices which have patella cartilage is 0.978. The distribution of dice coefficient is also relatively concentrated, which shows that the network can effectively segment the cartilage under normal circumstances. Table II shows the average validation dice coefficient (F1) and intersection over union (IoU) of our model. The average validation dice coefficient of femoral cartilage is 0.79 and the average validation IoU is 0.74, the average validation dice coefficient of the tibia is 0.85 and the average validation IoU is 0.78 and for patella cartilage, the average validation dice coefficient is 0.82 and the average validation IoU is 0.73. The reason of low validation F1 score from training F1 scores is that in the evaluation process of validation datasets, some slices in datasets have no cartilage.

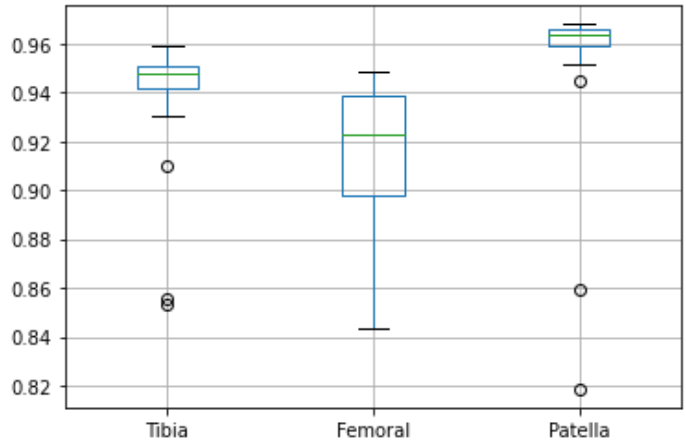

Fig. 4. Boxplot of dice-coefficient of those slices having cartilage from PSU-Net.

TABLE II. AVERAGE VALIDATION DICE-COEFFICIENT(F1) AND INTERSECTION OVER UNION(IOU) SCORES OF DIFFERENT CARTILAGES USING PSU-NET

Performance Metrics	Femoral	Tibia	Patella
F1	0.79	0.85	0.82
IoU	0.74	0.78	0.73

This article also compares proposed model with the U-Net, Branch residual U-Net (BRUNet) based on dilated convolution [35] and FU-Net [36] with batch normalization and residual block. Table III describes the dice coefficients of the four networks, which automatically segment femoral, tibia and patella cartilages. Compared with other segmentation models, the dice coefficients of knee cartilages have improved to a certain extent in PSU-Net, which shows that the model can segment knee cartilages more effectively. This is mainly because the proposed Squeeze and Excitation block with residual connection reduces the loss of feature information during propagation to a certain extent. At the same time, the proposed block increases the weights of useful features of the image and improves the segmentation performance in consequence.

Fig. 5 shows the segmentation results on some image slices from the test dataset. The first column is the slices of knee image from the test datasets, the second column is the label mask manually annotated, which provides the ground-truth, and the third column is the prediction result of the cartilage area by the PSU-Net. The green area represents femoral cartilage, the yellow area represents tibia cartilage, and the pink area shows patella cartilage. The first to fourth rows show a simple situation. When the knee image slices show different cartilages, our model outperforms contemporary models in segmenting different type of cartilage in input image slice. However, in some slices when the cartilage boundary is closely in contact with other organs like meniscus and tissue, then the segmentation performance of our model becomes weak as shown in the first column, the reason is that assigning weights in such condition becomes difficult. Fig. 6 shows the predicted axial 3D view of cartilage using Slicer software for two test datasets.

TABLE III. COMPARISON OF DICE-COEFFICIENT SCORE USING DIFFERENT MODELS FOR TWO TEST DATASETS AFTER TRAINING

Models	Femoral	Tibia	Patella
U-Net	0.80	0.76	0.84
FU-Net	0.82	0.80	0.87
BRUNET	0.77	0.73	0.78
PSU-Net	**0.86**	**0.89**	**0.85**

VII. CONCLUSION

In this paper, the improved network PSU-Net is proposed to automatically segment the femoral, tibia and patella cartilage in the knee MR image. The proposed model has employed Squeeze and Excitation block with residual connection instead of only convolution layer in U-Net to learn the feature information of the image more effectively. In order to reduce the problem of imbalance between the background and the bone area in the image, the image is clipped before training. In the training, a weighted loss function is used to optimize the model, and the weight of femoral, tibia and patella is increased to improve the cartilage segmentation. Our proposed model has achieved good segmentation results of each cartilage on the test datasets compared to other variants of U-Net models. The authors have noticed that proposed model clearly outperforms U-Net and other variants of U-Nets in segmenting the cartilages of femoral, tibia and Patella of the knee with Dice-Coefficient of 0.86, 0.89 and 0.85, respectively. PSU-Net can quickly and accurately segment femoral, tibia and patella, which help physicians to adjust treatment plans according to the condition. Detection and segmentation of cartilages in knee Image based on deep learning requires a large amount of training data. However, due to the limitation of segmentation targets, the number of annotated datasets in the Knee image group is small, which limits the effect of model training. As the number of publicly available annotated Knee images increases in the future, the segmentation performance of the proposed network will also be further improved. The segmentation of those cartilages whose boundary are in contact with meniscus or other tissues, are hard to be segmented by our model, is suggested in the future part of this work. Additionally, augmentation of data using generative model will also finish the problem of less data in medical images that will affect the segmentation results of the potential models.

ACKNOWLEDGMENT

The authors would like to express their sincere gratitude to University Kuala Lumpur (UniKL) for its generous support in funding this research project under the UniKL Excellent Research Grant Scheme (UniKL/CoRI/UER21013).

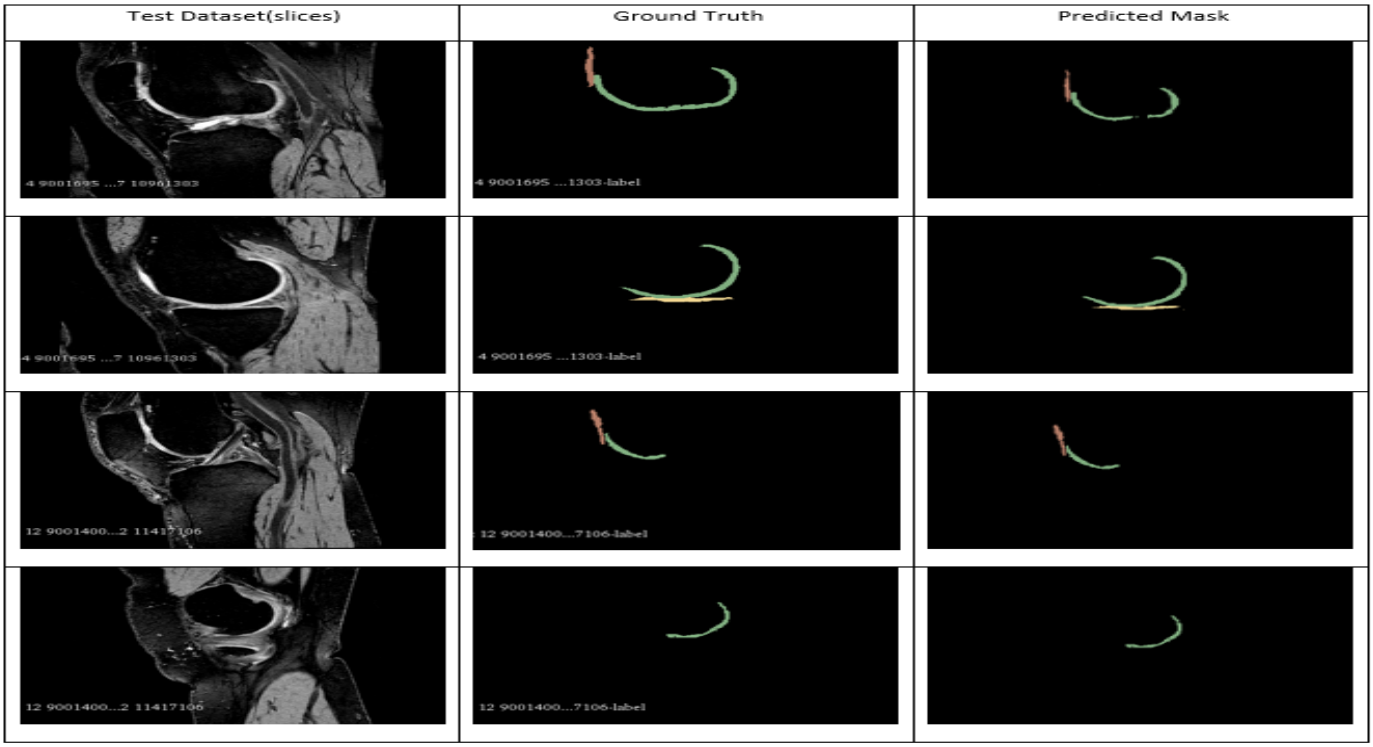

Fig. 5. Input knee image with manually annotated Groundtruth and predicted segmentation mask using PSU-Net.

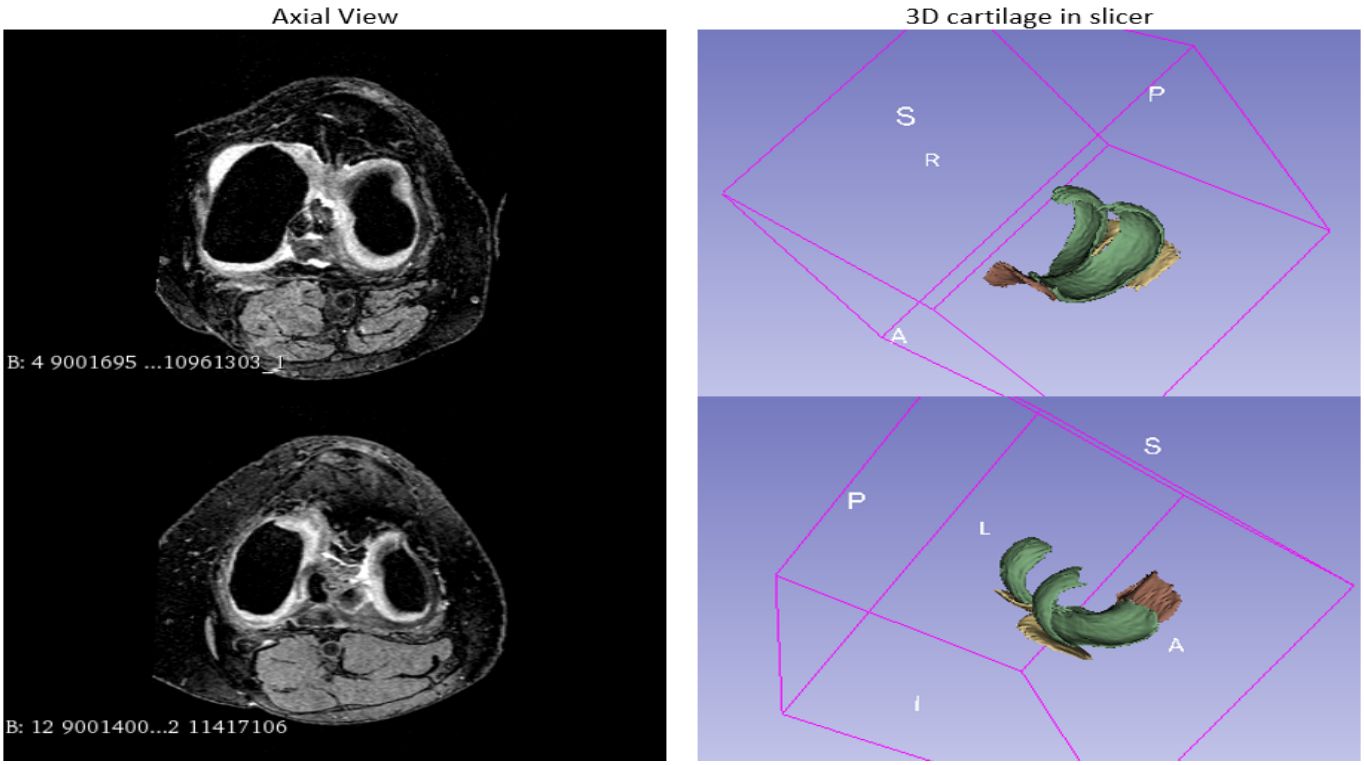

Fig. 6. Axial view of two test datasets and their predicted 3D segmented cartilage using PSU-Net.

REFERENCES

[1] Prathap Kumar, J., Arun Kumar, M., & Venkatesh, D. (2020). Healthy gait: Review of anatomy and physiology of knee joint. International Journal of Current Research and Review, 12(6), 1-8.

[2] Mahendrakar, Pavan, et al. "A Survey on Morphological Assessment of Knee Articular Cartilage from MR Images." 2018 International Conference on Smart Systems and Inventive Technology (ICSSIT). IEEE, 2018.

[3] Khokhlova, L., Komaris, D. S., Davarinos, N., Mahalingam, K., O'Flynn, B., & Tedesco, S. (2023). Non-invasive Assessment of Cartilage Damage of the Human Knee using Acoustic Emission Monitoring: a Pilot Cadaver Study. IEEE Transactions on Biomedical Engineering.

[4] Du, Yaodong, et al. "Knee osteoarthritis severity level classification using whole knee cartilage damage Index and ANN." Proceedings of the 2018 IEEE/ACM International Conference on Connected Health: Applications, Systems and Engineering Technologies. 2018.

[5] Teoh, Y. X., Lai, K. W., Usman, J., Goh, S. L., Mohafez, H., Hasikin, K., ... & Dhanalakshmi, S. (2022). Discovering knee osteoarthritis imaging features for diagnosis and prognosis: Review of manual imaging grading and machine learning approaches. Journal of healthcare engineering, 2022.

[6] Gan, H. S., Ramlee, M. H., Wahab, A. A., Lee, Y. S., & Shimizu, A. (2021). From classical to deep learning: review on cartilage and bone segmentation techniques in knee osteoarthritis research. Artificial Intelligence Review, 54(4), 2445-2494.

[7] Kumar, Dileep, et al. "Knee articular cartilage segmentation from MR images: A review." ACM Computing Surveys (CSUR) 51.5 (2018): 1-29.

[8] Siregar, S., Utami, P. R., Anuar, T. S., Nurfajri, A., & Saputri, W. A. (2023). Comparison of Nitrogen Levels in Normal Faeces and Faeces Infected by Ascaris Lumbricoides and Trichuris Trichiura. Journal of Advanced Research in Applied Sciences and Engineering Technology, 30(2), 13-18.

[9] Patil, P., & Patil, K. (2023). A Review on Disease Prediction using Image Processing. Journal Electrical and Computer Experiences, 1(1), 18-28.

[10] Hesamian, M. H., Jia, W., He, X., & Kennedy, P. (2019). Deep learning techniques for medical image segmentation: achievements and challenges. Journal of digital imaging, 32, 582-596.

[11] Melouah, A., & Layachi, S. (2018). Overview of Automatic seed selection methods for biomedical images segmentation. INTERNATIONAL ARAB JOURNAL OF INFORMATION TECHNOLOGY, 15(3), 499-504.

[12] Bhowmik, M. K., Das, K., & Bhattacharjee, D. (2019). Temperature profile guided segmentation for detection of early subclinical inflammation in arthritis knee joints from thermal images. Infrared Physics & Technology, 99, 102-112.

[13] Riza, S., Marlinawati, D., & Fahmi, M. A. M. (2019). COMSeg technique for MRI knee cartilage segmentation. International Review of Applied Sciences and Engineering, 10(2), 147-155.

[14] Almajalid, R., Zhang, M., & Shan, J. (2022). Fully automatic knee bone detection and segmentation on three-dimensional MRI. Diagnostics, 12(1), 123.

[15] Waqas, Nawaf, et al. "DEEPFAKE Image Synthesis for Data Augmentation." IEEE Access 10 (2022): 80847-80857.

[16] Xiao, H., Li, L., Liu, Q., Zhu, X., & Zhang, Q. (2023). Transformers in medical image segmentation: A review. Biomedical Signal Processing and Control, 84, 104791.

[17] Jiang, H., Diao, Z., Shi, T., Zhou, Y., Wang, F., Hu, W., ... & Yao, Y. D. (2023). A review of deep learning-based multiple-lesion recognition from medical images: classification, detection and segmentation. Computers in Biology and Medicine, 106726.

[18] Burton II, W., Myers, C., & Rullkoetter, P. (2020). Semi-supervised learning for automatic segmentation of the knee from MRI with convolutional neural networks. Computer methods and programs in biomedicine, 189, 105328.

[19] Ronneberger, Olaf, Philipp Fischer, and Thomas Brox. "U-net: Convolutional networks for biomedical image segmentation." Medical Image Computing and Computer-Assisted Intervention–MICCAI 2015: 18th International Conference, Munich, Germany, October 5-9, 2015, Proceedings, Part III 18. Springer International Publishing, 2015.

[20] Liu, F., Zhou, Z., Jang, H., Samsonov, A., Zhao, G., & Kijowski, R. (2018). Deep convolutional neural network and 3D deformable approach for tissue segmentation in musculoskeletal magnetic resonance imaging. Magnetic resonance in medicine, 79(4), 2379-2391.

[21] Zhou, Z., Zhao, G., Kijowski, R., & Liu, F. (2018). Deep convolutional neural network for segmentation of knee joint anatomy. Magnetic resonance in medicine, 80(6), 2759-2770.

[22] Ambellan, F., Tack, A., Ehlke, M., & Zachow, S. (2019). Automated segmentation of knee bone and cartilage combining statistical shape knowledge and convolutional neural networks: Data from the Osteoarthritis Initiative. Medical image analysis, 52, 109-118.

[23] Yi, X., Walia, E., & Babyn, P. (2019). Generative adversarial network in medical imaging: A review. Medical image analysis, 58, 101552.

[24] Hu, Z., Zhang, J., & Ge, Y. (2021). Handling vanishing gradient problem using artificial derivative. IEEE Access, 9, 22371-22377.

[25] Shafiq, M., & Gu, Z. (2022). Deep residual learning for image recognition: A survey. Applied Sciences, 12(18), 8972.

[26] Hu, Jie, Li Shen, and Gang Sun. "Squeeze-and-excitation networks." Proceedings of the IEEE conference on computer vision and pattern recognition. 2018.

[27] Razmjoo, Alaleh, et al. "T2 analysis of the entire osteoarthritis initiative dataset." Journal of Orthopaedic Research® 39.1 (2021): 74-85.

[28] You, Y., Niu, Y., Sun, F., Huang, S., Ding, P., Wang, X., ... & Zhang, J. (2022). Three-dimensional printing and 3D slicer powerful tools in understanding and treating neurosurgical diseases. Frontiers in surgery, 9, 1030081.

[29] Moolayil, J., & Moolayil, J. (2019). An introduction to deep learning and keras. Learn Keras for Deep Neural Networks: A Fast-Track Approach to Modern Deep Learning with Python, 1-16.

[30] Raschka, S., & Mirjalili, V. (2019). Python machine learning: Machine learning and deep learning with Python, scikit-learn, and TensorFlow 2. Packt Publishing Ltd.

[31] Yaniv, Z., Lowekamp, B. C., Johnson, H. J., & Beare, R. (2019). Correction to: SimpleITK image-analysis notebooks: A collaborative environment for education and reproducible research. Journal of Digital Imaging, 32(6), 1118.

[32] Bisong, E., & Bisong, E. (2019). Matplotlib and seaborn. Building Machine Learning and Deep Learning Models on Google Cloud Platform: A Comprehensive Guide for Beginners, 151-165.

[33] Bisong, E., & Bisong, E. (2019). Introduction to Scikit-learn. Building Machine Learning and Deep Learning Models on Google Cloud Platform: A Comprehensive Guide for Beginners, 215-229.

[34] Harris, C. R., Millman, K. J., Van Der Walt, S. J., Gommers, R., Virtanen, P., Cournapeau, D., ... & Oliphant, T. E. (2020). Array programming with NumPy. Nature, 585(7825), 357-362.

[35] Piao, S., & Liu, J. (2019, November). Accuracy improvement of UNet based on dilated convolution. In Journal of Physics: Conference Series (Vol. 1345, No. 5, p. 052066). IOP Publishing.

[36] Jafari, Mina, et al. "FU-net: multi-class image segmentation using feedback weighted U-net." Image and Graphics: 10th International Conference, ICIG 2019, Beijing, China, August 23–25, 2019, Proceedings, Part II 10. Springer International Publishing, 2019.